Institute of Space and Aeronautical Science, University of Tokyo
Report No. 533, October 1975

Viscous Flow Around a Transversally Oscillating Elliptic Cylinder

By

Atsushi OKAJIMA*, Hiroyuki TAKATA** and Tsuyoshi ASANUMA

Summary: To furnish some fundamental information about viscous effects of flow on the aerodynamic characteristic of an elliptic cylinder, we numerically solve the Navier-Stokes equations for flow around both stationary and transversally oscillating elliptic cylinders at Reynolds numbers of $R_e=40$ and 80, and also measure aerodynamic forces and pressure acting on an elliptic cylinder in the range of Reynolds numbers $R_e=40$ to 20000. There is consequently seen a good agreement between the calculated results and the experimental ones for steady and unsteady aerodynamic parameters at Reynolds numbers $R_e=40$ and 80. On the basis of the numerical results we examine the time-variation of flow pattern around an elliptic cylinder, e.g. locations of stagnation points, and the experimental ones we discuss the effects of angle of attack, Reynolds number and oscillatory frequency on aerodynamic parameters.

INTRODUCTION

Some studies analyzing the viscous unsteady flow around the cylinder have been made by solving the basic equations of motion which include the viscous term. Moore (1955) performed a calculation for the unsteady boundary layer around an elliptic cylinder set at the stall angle of attack in an oscillatory air-flow in order to get its aerodynamic lift force curve. Wang (1966) analyzed the flow around an elliptic cylinder which starts impulsively at a certain angle of attack in a viscous fluid. He showed that the inception of stall strongly depends on the thickness ratio and the angle of attack of the cylinder but depends weakly on Reynolds number. The viscous effect on an oscillating flat plate in viscous uniform flow for which Reynolds number is very large, has also been studied by Chu (1962), and Shen and Crimi (1965) by the use of Oseen's approximation, but their results on the viscous correction do not agree with each other. Recently, Lugt and Haussling (1972) obtained numerical solutions for laminar incompressible fluid flow past a stationary elliptic cylinder with various angles of attack and studied the flow characteristics of vortex shedding.

The purpose of the present paper is to furnish some fundamental information on the viscous effect during unsteady flow phenomena. This is accomplished by studying the behavior of viscous flow around an oscillating

* Research Institute for Applied Mechanics, Kyushu University, Fukuoka, Japan.
** Department of Aeronautics, University of Tokyo, Tokyo, Japan.

elliptic cylinder, first by means of a numerical solution of the Navier-Stokes equations. The application of the numerical calculation, however, is limited to rather low Reynolds number. Furthermore, there seems to be no information about how the results of numerical analysis for low Reynolds number can be extended to the case of higher Reynolds number. So, some experiments have been carried out to study the viscous flow around an oscillating elliptic cylinder, not only to confirm the validity of the present method of numerical calculation but also to provide information over a wide range of Reynolds number.

The latter half of this paper gives the experimental results for the fluctuating nomal force, moment and pressure acting on an ellipting cylinder which is subjected to a forced transversal oscillation with specified amplitude and frequency in the range of Reynolds number $R_e=40$ to 20000.

2. Numerical Calculation

2-1. Basic equations and boundary conditions

We consider an elliptic cylinder oscillating transversally in uniform viscous flow. The method of numerical solution used here is essentially that for a circular cylinder as reported in an earlier paper, Okajima, Takata and Asanuma (1975), so that we will briefly describe here only its essential features.

The equations of motion are developed in the system of elliptic coordinates (ξ, η), for one of the ξ-ordinate, ξ_0 forms the surface of the elliptic cylinder. The following relations exist between the (ξ, η)-coordinate system and the Cartesian coordinate system (x, y):

$$x=\cosh\xi\cos\eta, \qquad y=\sinh\xi\sin\eta \tag{1}$$

where the forcal distance of this coordinates is taken to be a unity, so the chord length c of the elliptic cylinder is $2\cosh\xi_0$.

When the elliptic cylinder moves with a velocity $A_y(t)$ transversally, or in the y-direction of Cartesian coordinates (x, y), we adopt the moving coordinate system fixed to the oscillating cylinder and then we express the Navier-Stokes equations and the continuity equation in this moving coordinate system (ξ, η) as follows:

$$\begin{aligned}
&\frac{\partial q_\xi}{\partial t}+\frac{q_\xi}{h}\frac{\partial q_\xi}{\partial \xi}+\frac{q_\eta}{h}\frac{\partial q_\xi}{\partial \eta}+\frac{q_\xi q_\eta}{h^2}\frac{\partial h}{\partial \eta}-\frac{{q_\eta}^2}{h^2}\frac{\partial h}{\partial \xi}+\frac{1}{h}\frac{\partial y}{\partial \xi}\frac{\partial A_y}{\partial t}\\
&\quad=-\frac{1}{\rho h}\frac{\partial p}{\partial \xi}-\frac{\nu}{h}\frac{\partial \zeta}{\partial \eta}\\
&\frac{\partial q_\eta}{\partial t}+\frac{q_\xi}{h}\frac{\partial q_\eta}{\partial \xi}+\frac{q_\eta}{h}\frac{\partial q_\eta}{\partial \eta}+\frac{q_\xi q_\eta}{h^2}\frac{\partial h}{\partial \xi}-\frac{{q_\xi}^2}{h^2}\frac{\partial h}{\partial \eta}+\frac{1}{h}\frac{\partial y}{\partial \eta}\frac{\partial A_y}{\partial t}\\
&\quad=-\frac{1}{\rho h}\frac{\partial p}{\partial \eta}+\frac{\nu}{h}\frac{\partial \zeta}{\partial \xi}
\end{aligned} \tag{2}$$

$$\frac{\partial(hq_\xi)}{\partial\xi}+\frac{\partial(hq_\eta)}{\partial\eta}=0 \tag{3}$$

and

$$\frac{\partial\zeta}{\partial t}+\frac{q_\xi}{h}\frac{\partial\zeta}{\partial\xi}+\frac{q_\eta}{h}\frac{\partial\zeta}{\partial\eta}=\frac{\nu}{h^2}\left(\frac{\partial^2\zeta}{\partial\xi^2}+\frac{\partial^2\zeta}{\partial\eta^2}\right) \tag{4}$$

where q_ξ and q_η are the velocity components of the ξ- and η-directions respectively, p is pressure, ρ is fluid density, ν is kinematic coefficient of viscosity, t is time, h is defined as $h=\sqrt{\cosh^2\xi-\cos^2\eta}$, the vorticity ζ as $(\partial(hq_\eta)/\partial\xi-\partial(hq_\xi)/\partial\eta)/h^2$ and the oscillatory velocity $A_y(t)$ is given as $2\pi f\delta\sin 2\pi ft$, f denoting the imposed frequency and δ the amplitude of the oscillatory displacement.

Introducing the stream function ψ defined by

$$hq_\xi=\partial\psi/\partial\eta, \qquad hq_\eta=-\partial\psi/\partial\xi,$$

we may rewrite equation (4) as follows:

$$\frac{\partial\zeta}{\partial t}+\frac{1}{h^2}\left(\frac{\partial\psi}{\partial\eta}\frac{\partial\zeta}{\partial\xi}-\frac{\partial\psi}{\partial\xi}\frac{\partial\zeta}{\partial\eta}\right)=\frac{\nu}{h^2}\left(\frac{\partial^2\zeta}{\partial\xi^2}+\frac{\partial^2\zeta}{\partial\eta^2}\right) \tag{5}$$

with the continuity equation (3) automatically being satisfied.

For the sake of convenience, the stream function will be expressed by,

$$\psi=\psi_p+\tilde{\psi}$$

$$\psi_p=Ue^{\xi_0}\sinh(\xi-\xi_0)\left(\sin(\eta-\alpha)+\frac{2\pi f\delta}{U}\cos\eta\cdot\sin 2\pi ft\right) \tag{6}$$

where α is the angle of attack of the elliptic cylinder and U is the velocity of the free stream, which is taken to be a unity, here. ψ_p represents the stream function of potential flow around the elliptic cylinder and $\tilde{\psi}$ is the deviation of actual flow from the former ψ_p.

The vorticity ζ is given by

$$\frac{\partial^2\tilde{\psi}}{\partial\xi^2}+\frac{\partial\tilde{\psi}}{\partial\eta^2}=-h^2\zeta. \tag{7}$$

Equations (5) and (7) are the basic equations to be solved under the boundary conditions mentioned below. The boundary conditions to be satisfied on the surface ($\xi=\xi_0$) of an elliptic cylinder are that there be no cross flow through its surface and no slip flow along it, that is,

$$\psi_0=0, \qquad \left(-\frac{1}{h}\frac{\partial\psi}{\partial\xi}\right)_0=0, \tag{8}$$

where suffix 0 denotes the value on the surface, $\xi=\xi_0$.

As proposed by Okajima, Takata and Asanuma (1975) for the circular cylinder, we will impose the following condition upon a boundary $\xi=\xi_\infty$ sufficiently far from the cylinder instead of the infinite boundary:

$$\tilde{\psi}_\infty=A(\xi_\infty-\xi_0), \qquad \zeta_\infty=0, \tag{9}$$

where suffix ∞ denotes the value on the boundary outer edge, $\xi=\xi_\infty$, and A is the value determined by the implicit process at each time step in the numerical calculation.

2-2. Aerodynamic coefficients

Various aerodynamic coefficients can be obtained by the following method. We take the chord-length c of the cylinder and the velocity U of the free streem as units of length and volocity respectively, and reduce the aerodynamic parameters into non-dimensional forms. Reynolds number may be defined as $Re=Uc/\nu$ and reduced frequency as $k=2\pi fc/U$.

From equation (2) the coefficient of pressure on the surface ($\xi=\xi_0$) based on that at the trailing edge ($\xi=\xi_0$, $\eta=0$) may be obtained by

$$C_p(\eta)-C_p(0)=\frac{4\cosh\xi_0}{Re}\int_0^\eta\left(\frac{\partial\zeta}{\partial\xi}\right)_0 d\eta-\left(\frac{\delta}{c}\right)k^2\cdot\tanh\xi_0\cdot\sin\eta\cdot\cos 2\pi ft. \quad (10)$$

The coefficient of viscous shear stress on the surface is given by

$$C_\tau(\eta)=\frac{4\cosh\xi_0}{Re}\left(\frac{1}{h}\frac{\partial q_\eta}{\partial\xi}\right)_0=\frac{4\cosh\xi_0}{Re}\zeta_0. \quad (11)$$

The forces normal and tangential to the major axis and the moment about the midchord point of the cylinder consist of two components, namely, those due to pressure

$$\left.\begin{aligned} C_{NP}&=-\frac{1}{2}\int_0^{2\pi}C_p(\eta)\sin\eta d\eta,\\ C_{TP}&=-\frac{\tanh\xi_0}{2}\int_0^{2\pi}C_p(\eta)\cos\eta d\eta,\\ C_{MP}&=-\frac{1}{8\cosh^2\xi_0}\int_0^{2\pi}C_p(\eta)\sin 2\eta d\eta, \end{aligned}\right\} \quad (12)$$

and those due to viscous shear stress

$$\left.\begin{aligned} C_{NS}&=\frac{\tanh\xi_0}{2}\int_0^{2\pi}C_\tau(\eta)\cos\eta d\eta,\\ C_{TS}&=-\frac{1}{2}\int_0^{2\pi}C_\tau(\eta)\sin\eta d\eta,\\ C_{MS}&=-\frac{\tanh\xi_0}{4}\int_0^{2\pi}C_\tau(\eta)d\eta. \end{aligned}\right\} \quad (13)$$

Then coefficients of normal and tangential forces and moment are, respectively,

$$\left.\begin{aligned} C_N&=C_{NP}+C_{NS},\\ C_T&=C_{TP}+C_{TS},\\ C_M&=C_{MP}+C_{MS}. \end{aligned}\right\} \quad (14)$$

Further, only fluctuating components of the above aerodynamic parameters, which will be designated by the wave mark ($\sim$), are divided by the ratio (δ/c), to account for the amplitude of the oscillatory displacement of the cylinder.

2-3. Numerical procedure

In the numerical calculation the flow field is divided into a number of finite discrete meshes. The rapid changes of the stream function and the vorticity of flow near the cylinder in the vicinity of the leading and trailing edges, require small mesh size, while in the field far from the cylinder rather large mesh size may be used. This gradation of mesh size is conveniently achieved by transforming the physical plane into the elliptic coordinates (ξ, η), which are divided into a finite discrete mesh of points (iS, jS) with a constant mesh size S. In addition, the mesh is reduced further close to the cylinder by dividing the radial mesh by two $(S/2)$. This method has already been found to be desirable for accuracy and economy of computation as indicated by Okajima, Takata and Asanuma (1975). However, all expressions of a finite difference in the following are obtained in the field (iS, jS) divided with a constant mesh size S, for convenience.

For a finite difference analogue to compute the vorticity $\zeta^{t+\Delta t}(i, j)$ at each discrete time $(t+\Delta t)$ from the known values of the stream function $\psi^t(i, j)$ and the vorticity $\zeta^t(i, j)$ at time t, we use implicit process because of its computational stability. Replacing the vorticity equation (5) by difference expression gives:

$$\frac{\zeta^{t+\Delta t}(i, j)-\zeta^t(i, j)}{\Delta t}=\frac{2}{Re}\left(\frac{1}{2}\nabla^2\zeta^{t+\Delta t}(i, j)+\frac{1}{2}\nabla^2\zeta^t(i, j)\right)$$

$$+\frac{1}{16S^2h^2}(\zeta^{t+\Delta t}(i, j+1)+\zeta^t(i, j+1)-\zeta^{t+\Delta t}(i, j-1)-\zeta^t(i, j-1))$$

$$\times(\psi^{t+\Delta t}(i+1, j)+\psi^t(i+1, j)-\psi^{t+\Delta t}(i-1, j)-\psi^t(i-1, j))$$

$$-\frac{1}{16S^2h^2}(\zeta^{t+\Delta t}(i+1, j)+\zeta^t(i+1, j)-\zeta^{t+\Delta t}(i-1, j)-\zeta^t(i-1, j))$$

$$\times(\psi^{t+\Delta t}(i, j+1)+\psi^t(i, j+1)-\psi^{t+\Delta t}(i, j-1)-\psi^t(i, j-1)) \qquad (15)$$

where $\psi^t(i, j)=\psi_p{}^t(i, j)+\tilde{\psi}^t(i, j)$,

$$\nabla^2\zeta^t(i, j)=\frac{1}{S^2h^2}(\zeta^t(i, j+1)+\zeta^t(i, j-1)+\zeta^t(i+1, j)+\zeta^t(i-1, j)-4\zeta^t(i, j)),$$

and $1\leqq j\leqq N$, $1\leqq i\leqq M$.

Next, equation (7) for $\tilde{\psi}(i, j)$ which corresponds to $\zeta(i, j)$ as indicated above, may be solved by the successive line over-relaxation method which is employed along the lines $\xi=$constant, sweeping from $\xi=\xi_0$ (on the surface of the cylinder) to $\xi=\xi_\infty$ (on the outer edge of the computational domain). The finite difference approximation of equation (7) is,

$$\tilde{\psi}^{K+1}(i, j)=\tilde{\psi}^K(i, j)+\omega(\tilde{\psi}^{K+1*}(i, j)-\tilde{\psi}^K(i, j)), \qquad (16)$$

where

$$\tilde{\psi}^{K+1*}(i, j)=\frac{1}{4}(\tilde{\psi}^{K}(i+1, j)+\tilde{\psi}^{K+1}(i-1, j)+\tilde{\psi}^{K+1*}(i, j+1)$$
$$+\tilde{\psi}^{K+1*}(i, j-1)+S^2h^2(i, j)\zeta(i, j)),$$

and the superscript K indicates the value of the Kth iteration. The optimum accelaration parameter ω is 1.4, which is found after several trials. The boundary conditions for $\tilde{\psi}$ and ζ are as follows: on the surface of the cylinder $(i=1)$,

$$\tilde{\psi}(1, j)=0, \qquad \zeta(1, j)=-\frac{2(\psi(2, j)-\psi(1, j))}{S^2h^2(1, j)}, \tag{17}$$

and on the boundary sufficiently far from the cylinder $(i=M)$,

$$\tilde{\psi}(M, j)=A(\xi_\infty-\xi_0), \qquad \zeta(M, j)=0, \tag{18}$$

where

$$A=-\frac{1}{SN}\sum_{j=1}^{N}(\tilde{\psi}(M, j)-\tilde{\psi}(M-1, j)),$$

and this value may be determined by the implicit method. The procedure for solving these equations (15) and (16) under the boundary conditions given by equations (17) and (18) is the same as that for a circular cylinder treaded in Okajima, Takata and Asanuma (1975). Therefore, the detailed procedure used for the numerical calculations will be omitted here. In the case of an elliptic cylinder, we use a standard mesh with the parameter of computation $N=30$ or a mesh spacing $S=\pi/15$, for $Re=40$, and a fine mesh with a half-spacing $S_\xi=S/2$ in the ξ-direction only and $N=30$ for $Re=80$, with reference to the preliminary examination of the network in the case of a circular cylinder.

3. Results of Numerical Calculation

3-1. Case of a stationary elliptic cylinder

Fig. 1 shows the representative configurations of flow pattern and equi-vorticity lines around stationary elliptic cylinders with thickness ratios of 20% and 50% at angles of attack of $\alpha=0°$ and 15° and Reynolds number $Re=80$, for the almost steady state. To obtain these flow patterns, the calculations are carried on to the time when the aerodynamic parameters scarcely change with time, taking inviscid potential flow as the initial condition. At angle of attack of $\alpha=0°$, the separation of the boundary layer can not be observed on the surface of the elliptic cylinder with the 20% thickness ratio. On the elliptic cylinder with the 50% thickness ratio, however, the boundary layers separate from the surface and a pair of standing vortices appear just as for the case of a stationary circular cylinder. In the

case of the elliptic cylinder with the thickness ratio, the separation of the boundary layer is not observed even at $\alpha=15°$, and it should be noted that in spite of the rounded trailing edge of the elliptic cylinder and such small Reynolds number as 40 or 80, the point of downstream stagnation essentially remains at the trailing edge just as the Kutta condition is satisfied on an aerofoil with a sharp trailing edge, as shown in Fig. 1 (a). On the other hand, in the case of the 50% elliptic cylinder at $\alpha=15°$, the boundary layers separate on both the upper and the lower surfaces and the Karman vortex street is shed alternately behind the stationary cylinder as shown in Fig. 1 (b). This figure shows the flow pattern at the time $t=22.75$, that is, the time elapsed after the abrupt start of the cylinder and reduced in the non-dimensional form by the uniform velocity/the focal distance of the elliptic cylinder. The unsymmetry of flow around the elliptic cylinder with the angle of attack seems to cause the Karman vortex street to appear in wake. The Strouhal number $St_K(=f_Kc/U)$ related to the chord-length c is detected to be about 0.17 from the fluctuation of the lift force induced by the Karman vortex street, where f_K is the frequency.

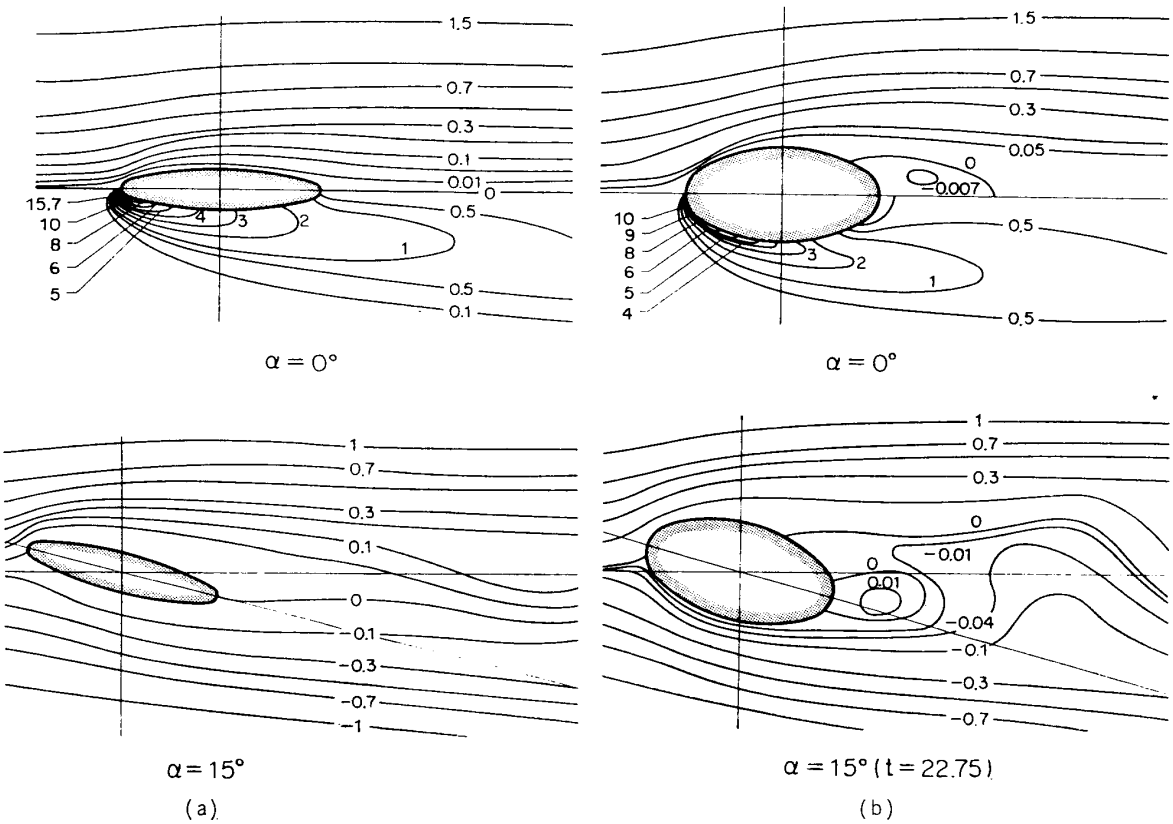

(a) (b)

FIG. 1. Stream lines and equi-vorticity lines of the stationary elliptic cylinder with the thickness ratios of 20% and 50%.

(a) $Re=80$, $\alpha=0°$ (the upper side: stream lines and the lower side: equivorticity lines) and $\alpha=15°$ (stream lines), and the thickness ratio of 20%.

(b) $Re=80$, $\alpha=0°$ (the upper side: stream lines and the lower side: equivorticity lines) and $\alpha=15°$ (stream lines), and the thickness ratio of 50%.

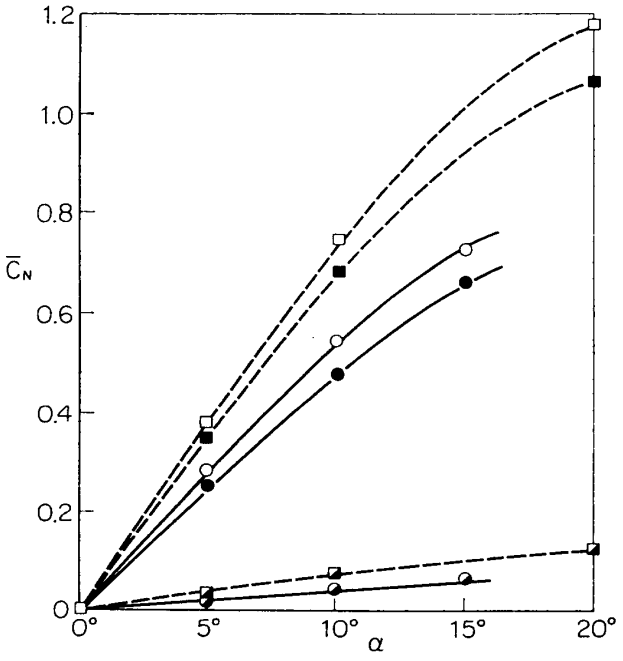

(a) Normal force

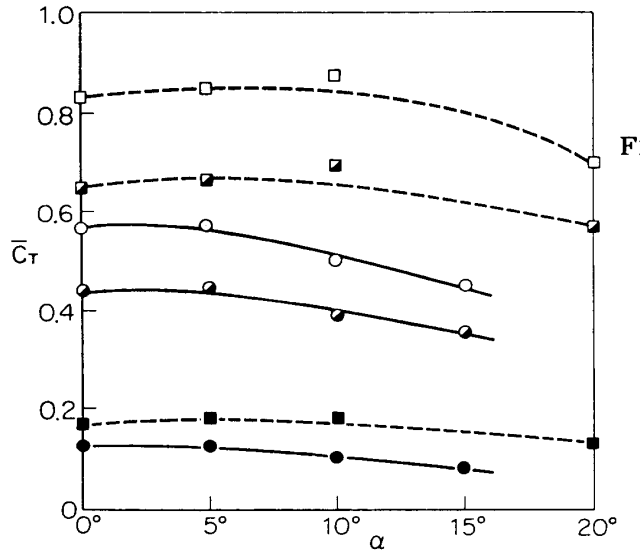

(b) Tangential force

FIG. 2-1. Normal and tangential forces and moment of the stationary elliptic cylinder with the thickness ratio of 20% at $Re=40$ and 80.
The components due to pressure: --■--, $Re=40$; -●-, $Re=80$. The components due to viscous shear stress: --◪--, $Re=40$; -◕-, $Re=80$. The resultant: --□--, $Re=40$; -○-, $Re=80$. The distance $\bar{x}_a$ denotes the chordwise position of the aerodynamic center: --⊡--, $Re=40$; -⊙-, $Re=80$.

The steady aerodycamic forces $\bar{C}_N$, $\bar{C}_T$, respectively, normal and tangential to the major axis of the cylinder and the moment $\bar{C}_M$ about the midchord are plotted against the angle of attack α in Fig. 2. With an increase in the angle of attack α, the normal force $\bar{C}_N$ and the moment $\bar{C}_M$ become large monotonically, and about 90% of these forces consists of the component due to pressure, even at such low Reynolds number as 40 or 80. The tangential forces $\bar{C}_T$, however, contains about 80% component due to viscous shear stress. The values of $\bar{C}_N$, $\bar{C}_T$, and $\bar{C}_M$ for $Re=80$ are smaller than those for $Re=40$. This tendency is similar to the result obtained in the analysis by Miyagi (1964) using Oseen's approximation. The chordwise

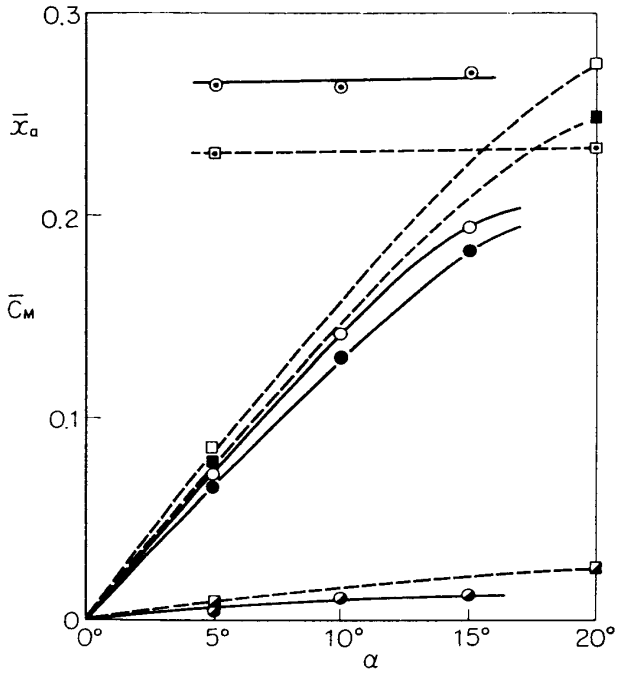

(c) Moment and aerodynamic center

FIG. 2-2. Normal and tangential forces and moment of the stationary elliptic cylinder with the thickness ratio of 20% at $Re=40$ and 80.
The components due to pressure: --■--, $Re=40$; -●-, $Re=80$. The components due to viscous shear stress: --◪--, $Re=40$; -◔-, $Re=80$. The resultant: --□--, $Re=40$; -○-, $Re=80$. The distance $\bar{x}_a$ denotes the chordwise position of the aerodynamic center: --⊡--, $Re=40$; -⊙-, $Re=80$.

position of the aerodynamic center is near the quater-chord point and moves forward with an increase of Reynolds number as in Fig. 2 (c).

3-2. Case of a transversally oscillating elliptic cylinder

(a) Case of elliptic cylinder with thickness ratio of 20%

We consider the elliptic cylinder oscillating transversally in uniform viscous flow. Fig. 3 illustrates the calculated results of the oscillating elliptic cylinder under the condition of Reynolds number $Re=40$, reduced frequency $k=1.0$, amplitude of displacement chord-length ratio, $\delta/c=4\%$ and angle of attack $\alpha=0°$. We take viscous flow around the stationary cylinder as the initial condition for this calculation. This corresponds to the cylinder beginning to oscillate in uniform viscous flow. The periodic oscillation of the cylinder is seen not to greatly change the flow around it, so that the flow pattern around the oscillating cylinder is shown only at the time 22.4 in Fig. 3 (a), and the point of downstream stagnation remains almost in the vicinity of the trailing edge. As shown in Fig. 3 (b) and 3 (c), the fluctuating normal force and moment about the midchord point vary with time in a sinusoidal wave form with some phase difference $\phi_N=30°$ and $\phi_M=-1°$,

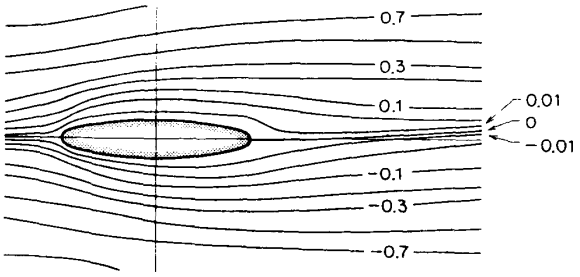

(a) Stream lines ($t=22.4$)

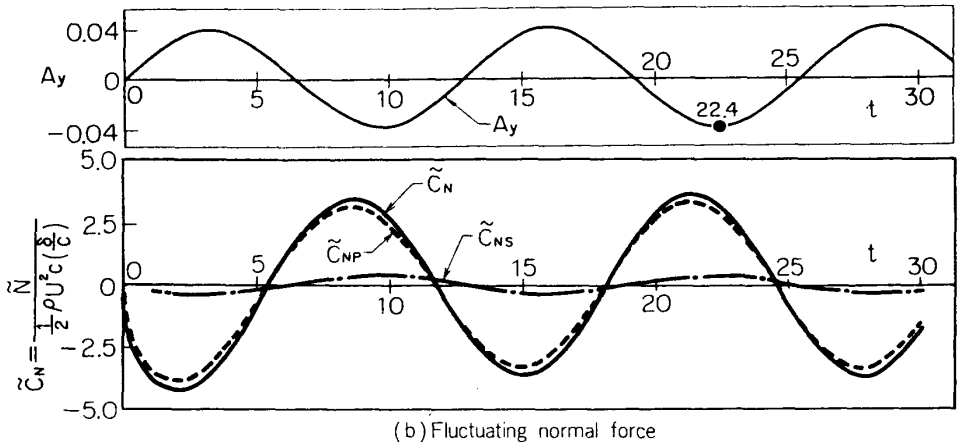

(b) Fluctuating normal force

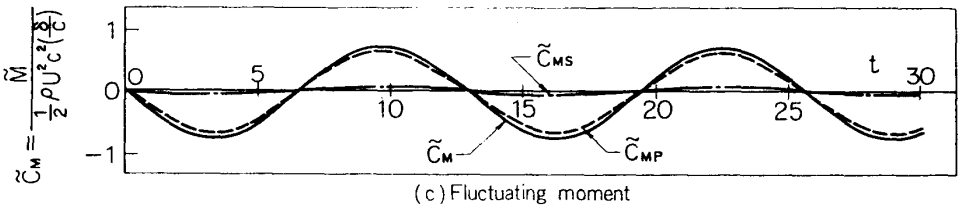

(c) Fluctuating moment

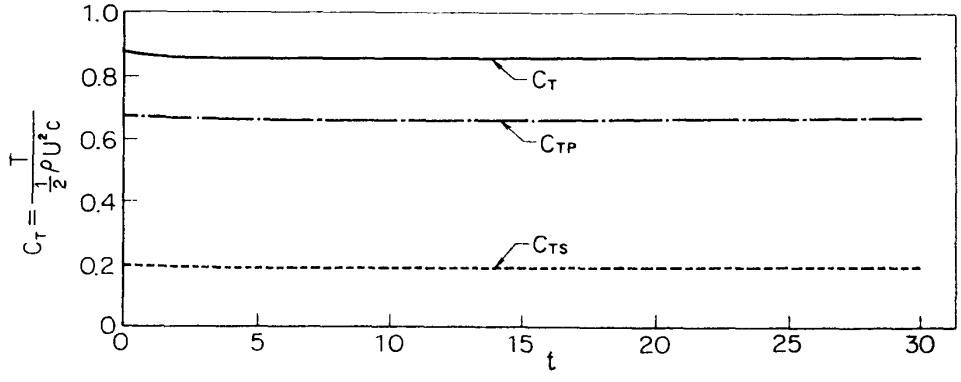

(d) Tangential force

FIG. 3. Stream lines, normal force, moment and tangential force of the transversally oscillating elliptic cylinder with the thickness ratio of 20% at $Re=40$, $\alpha=0°$, $k=1.0$ and $\delta/c=4\%$.

respectively from the assumed quasi-steady forces*. However, the tangential force C_T, 80% of which consists of the component due to viscous shear stress, remains at a constant value as in Fig. 3 (d) without being affected by the oscillation of the cylinder at all, so only this parameter need not be divided by the oscillatory amplitude δ/c. For the case of $Re=80$, $k=0.6$ and a high angle of attack of $\alpha=15°$, Fig. 4 shows that the fluctuating normal force acting on the cylinder is sinusoidal with a fairly constant amplitude $|\tilde{C}_N|=1.8$ and has some phase lead difference $\phi_N=23°$ relative to the motion of the cylinder. In this case we can also see a small attached eddy on the upper surface of the cylinder, repeatedly growing (at the time $t=16.0$ in Fig. 4 (a)) and disappearing.

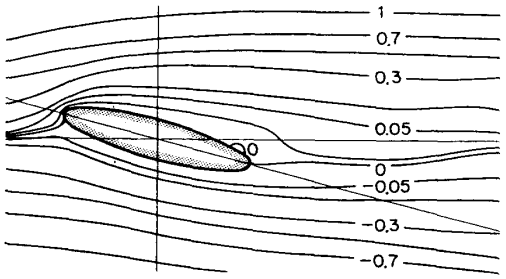

(a) Stream lines ($t=16.0$)

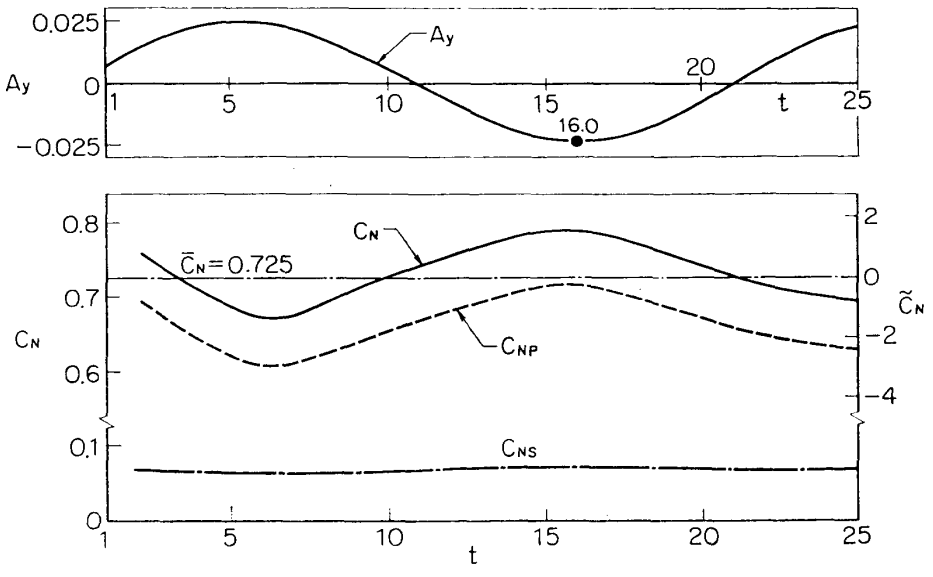

(b) Normal force

FIG. 4. Stream lines and normal force of the transversally oscillating elliptic cylinder with the thickness ratio of 20% at $Re=80$, $\alpha=15°$, $k=0.6$ and $\delta/c=4\%$.
——— denotes the value for the stationary cylinder. Only the fluctuating components of normal force $\tilde{C}_N$ are divided by the oscillatory amplitude δ/c.

* When the cylinder oscillates with very low frequency, the force exerted on it may be proportional to the oscillatory velocity with the opposite sign, i.e. $-Ay(t)$. So, we will use the variation of this quasi-steady force as the time basis.

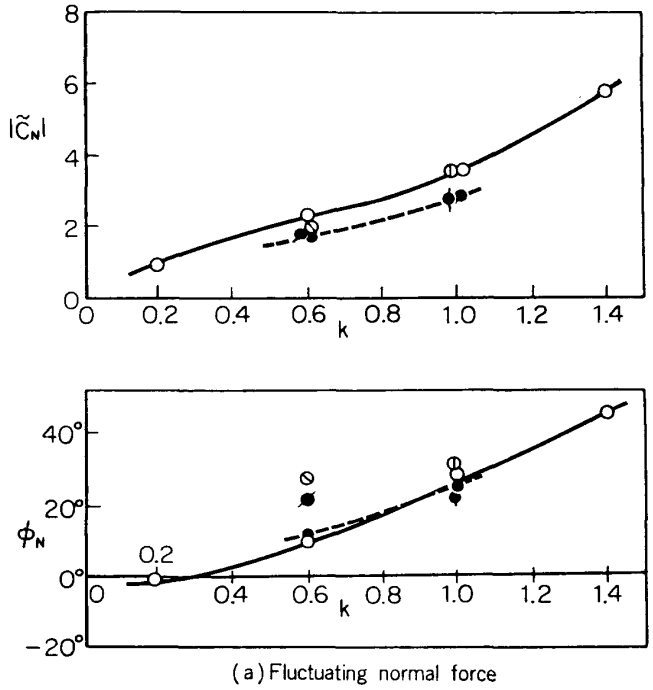

(a) Fluctuating normal force

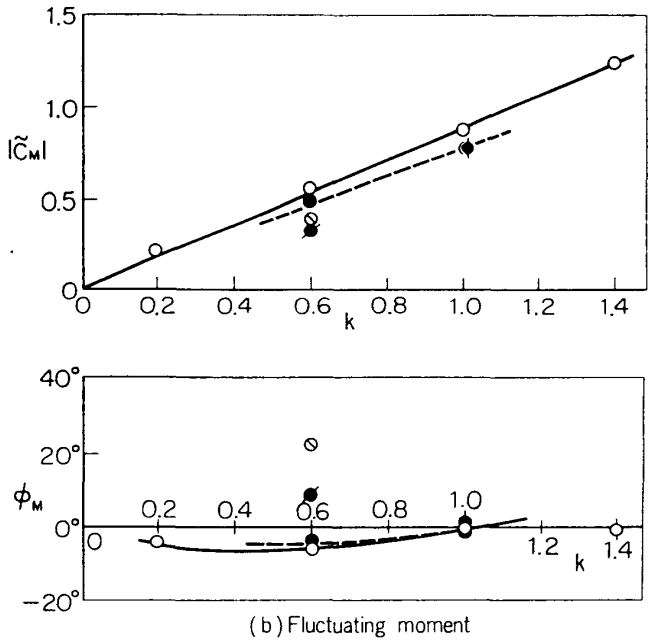

(b) Fluctuating moment

FIG. 5. The amplitudes and phases of fluctuating normal force and moment acting on the transversally oscillating elliptic cylinder with the thickness ratio of 20%, at $Re=40$ and 80 and $\delta/c=4\%$.
$Re=40$: -○-, $\alpha=0°$; ⊕, $\alpha=5°$; ⊘, $\alpha=20°$.
$Re=80$: --●--, $\alpha=0°$; ◖●◗, $\alpha=5°$; ◢●◣, $\alpha=15°$.

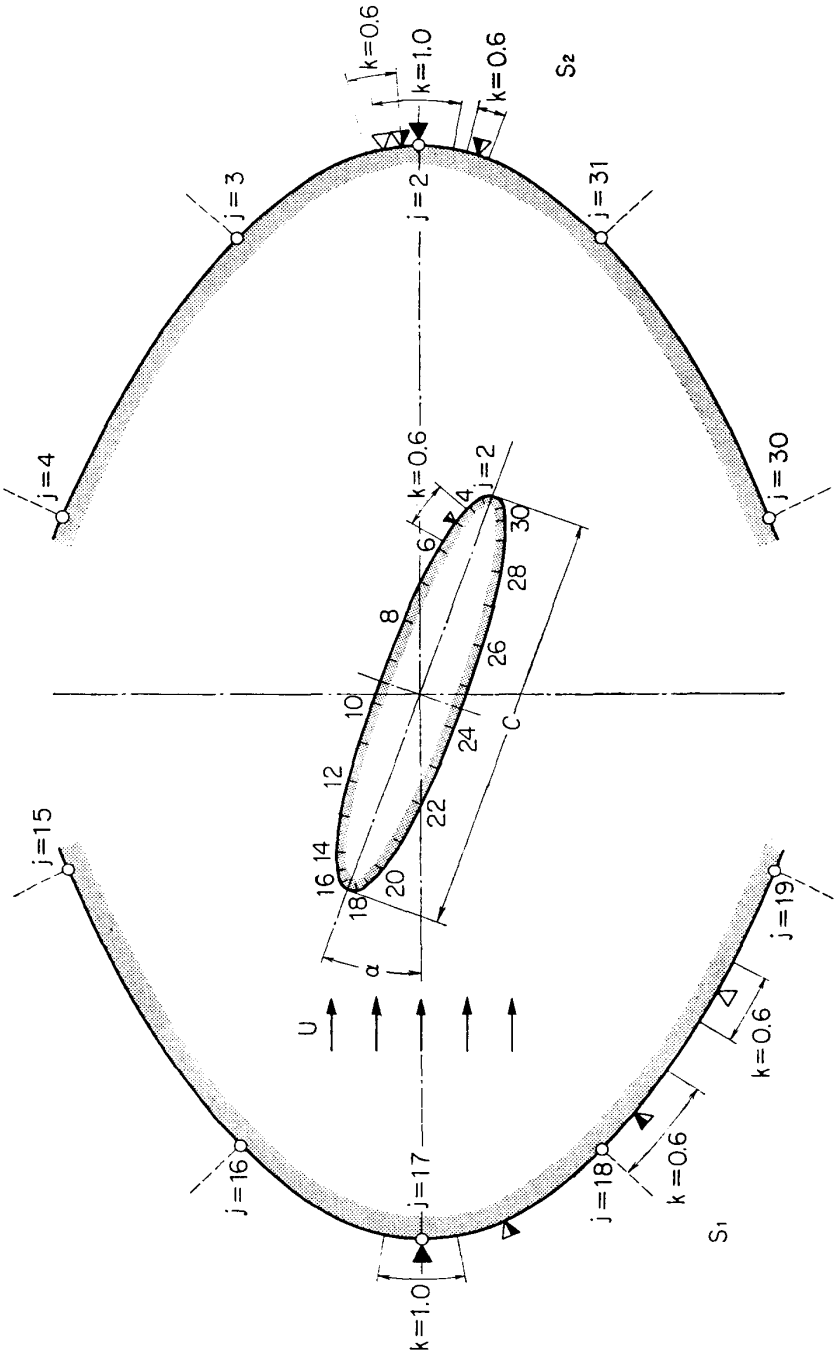

FIG. 6. The behaviours of up- and downstream points, S_1, S_2, respectively, where the viscous shear stress vanishes on the elliptic cylinder with the thickness ratio of 20%. The location of their points for the stationary cylinder: ▲◀, $Re=40$ and 80, $\alpha=0°$; ◺◀, $Re=40$, $\alpha=5°$; ◺◁, $Re=40$, $\alpha=20°$; ◣◀, $Re=80$, $\alpha=15°$. ↶ denotes the width of the movement of their points for the oscillating cylinder at various reduced frequencies.

Fig. 5 summarizes the calculated results of the fluctuating normal force and moment acting on the 20% elliptic cylinder against the reduced frequency k. It can be seen that with an increase in the reduced frequency the fluctuating normal force grows in amplitude and advances in phase, while an increase in the angle of attack does not have any great influence except on the phase lead. This figure also shows that an increase of Reynolds number from 40 to 80, makes the amplitude of the fluctuating normal force smaller. The reduction in the fluctuating normal force seems to be suggested by the steady normal force characteristics shown in Fig. 2.

Fig. 6 shows the locations of the up- and down-stream points, S_1, S_2 by the small triangles, where the viscous shear stress vanishes, that is, on the numerical calculation the stream function of the nearest lattice point from the cylinder surface is estimated to equal to zero by interpolation, for the 20% elliptic cylinder with the various angles of attack. In this figure, the vicinities of the leading and trailing edges are magnified so as to be shown in detail. The locations of these points may not be strictly accurate but are not different within the computational errors. It is seen on the stationary cylinder that the boundary layer does not separate and that an increase in the angle of attack causes the point of upstream stagnation to move farther away on the lower surface from the leading edge, and on the lower surface from the leading edge, and on the other hand, the point of downstream stagnation to remain in the narrow region around the trailing edge, in spite of the rounded trailing edge of the elliptic cylinder and such small Reynolds number as 40 or 80.

When this cylinder is transversally oscillating, these points move periodically about each location corresponding to that of the stationary cylinder, with the amplitude as shown by the arrows in Fig. 6. The amplitude of the downstream point is quite smaller than that of the upstream point.

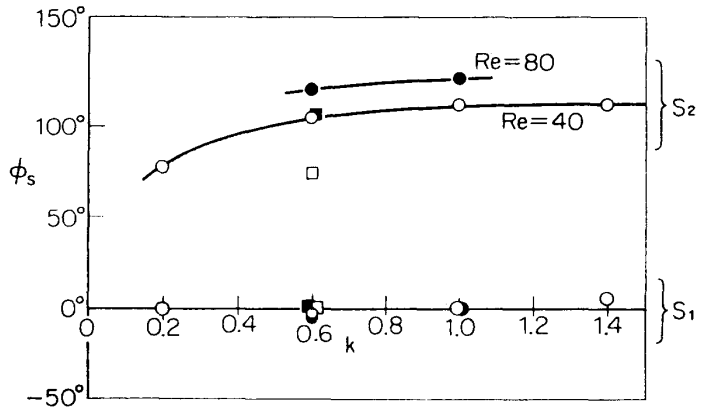

FIG. 7. The phase of the movement of the up- and downstream points, S_1, S_2, respectively, where the viscous shear stress vanishes on the transversally oscillating elliptic cylinder with the thickness ratio of 20% at Re=40 and 80. Re=40: -○-, α=0°; □, α=20°. Re=80: -●-, α=0°; ■, α=15°.

The upstream point S_1 moves almost in phase with the oscillatory velocity of the cylinder, i.e. $\phi_{S_1}\simeq 0°$ while the downstream point S_2 does likewise but with some phase difference relative to the oscillatory velocity, which is shown to be $\phi_{S_2}=110°\sim 130°$ ($k>0.5$) in Fig. 7. This may be explained by analyzing the calculated results. This analysis indicates that when the elliptic cylinder starts abruptly in still liquid at a certain angle of attack, the point of upstream point S_1 moves rapidly to its steady location, but that of the downstream S_2 which is first located on the upper surface, moves rather slowly to the region around the trailing edge. Therefore, on the oscillating cylinder, the upstream point S_1 may move almost in phase with the oscillatory velocity of the cylinder, while that of the downstream S_2 will follow but with some time delay.

(b) Case of elliptic cylinder with thickness ratio 50%

Next, Fig. 8 is a typical example of the flow around an elliptic cylinder oscillating with a large thickness ratio of 50%. This figure shows the flow

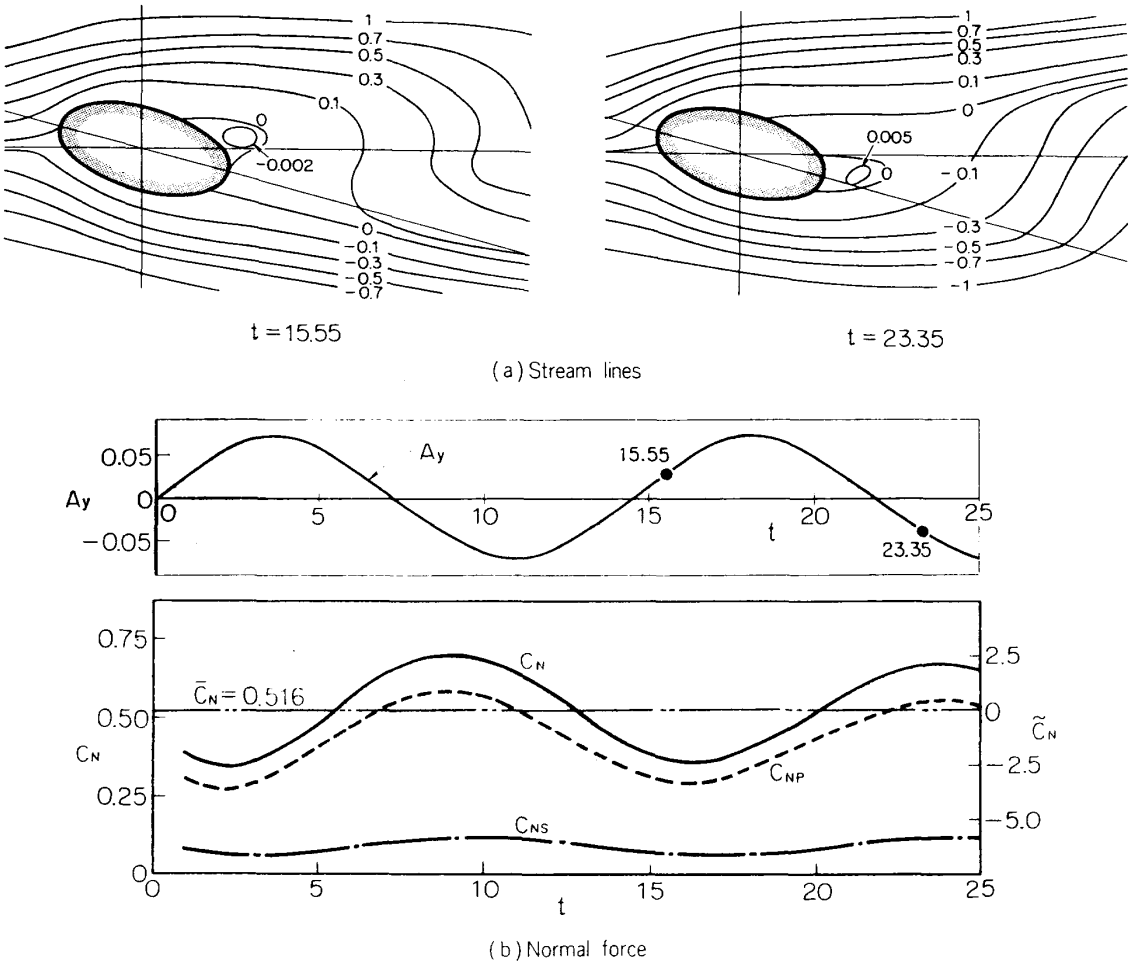

FIG. 8. Stream lines and normal force of the transversally oscillating elliptic cylinder with the thickness ratio of 50% at $Re=80$, $\alpha=15°$, $k=1.0$ and $\delta/c=10\%$. The interval between the time $t=15.55$ and $t=23.35$ is 0.61 times the period of the cylinder oscillation.

configurations at the time $t=15.55$ and $t=23.35$ when the almost maximum normal force is exerted down- and upward, respectively, on the cylinder which is subjected to the oscillation with the frequency $k=1.0$, the amplitude of displacement / the chord-length ratio, $\delta/c=10\%$ and the angle of attack $\alpha=15°$. In the flow patterns at these two times between which the interval is about a half period of the cylinder oscillation, the wakes behind the cylinder are observed to be arranged in the reverse shape, each other. It implies that the wake pattern is changing with the imposed frequency $k=1.0$. Therefore the normal force (and moment) of the cylinder also varies periodically with that frequency, as shown in Fig. 8 (b).

The fluctuating normal forces exerted on the 50% elliptic cylinder are summarized in Fig. 9, against the reduced frequency k at $Re=80$. The amplitude of the total normal force $|\tilde{C}_N|$ and the component part due to the pressure $|\tilde{C}_{NP}|$ become large as the reduced frequency k increases. The phase differences ϕ_N, ϕ_{NP}, ϕ_{NS} of $\tilde{C}_N$, $\tilde{C}_{NP}$, $\tilde{C}_{NS}$ are gradually leading with an increase in the reduced frequency. The value of the phase difference $\phi_{NP}=92°$ at $k=1.4$ means that the cylinder would be set in the aerodynamically unstable situation without the viscous component $\tilde{C}_{NS}$, which seems to be provoked by the so-called vortex excitation. The cylinder, however, is actually stable by the viscous effect.

For the elliptic cylinder with the 50% thickness ratio on which the boundary layer separates, the behaviour of the points S_1, S_2, S_3 and $S_{3'}$

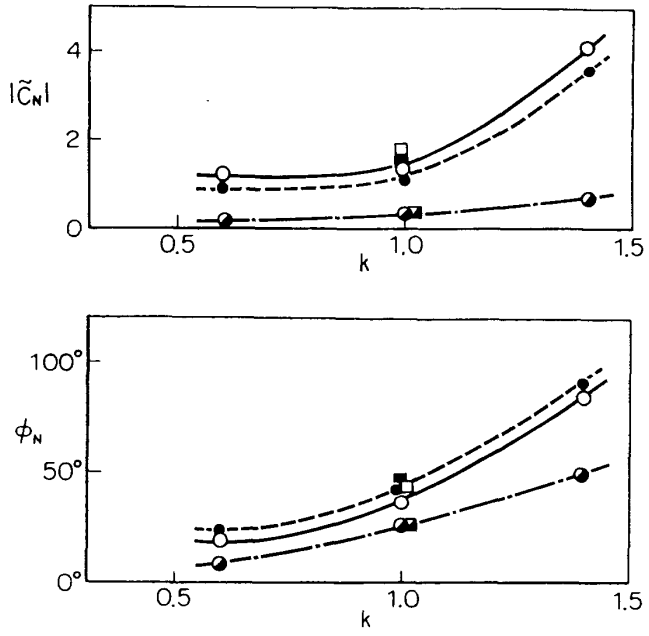

FIG. 9. The amplitudes and phases of the fluctuating normal force acting on the transversally oscillating elliptic cylinder with the thickness ratio of 50% at $Re=80$ and $\delta/c=10\%$.
$\alpha=0°$: -○-, $\tilde{C}_N$; --●--, $\tilde{C}_{NP}$; --◔--, $\tilde{C}_{NS}$.
$\alpha=15°$: □, $\tilde{C}_N$; ■, $\tilde{C}_{NP}$; ◪, $\tilde{C}_{NS}$.

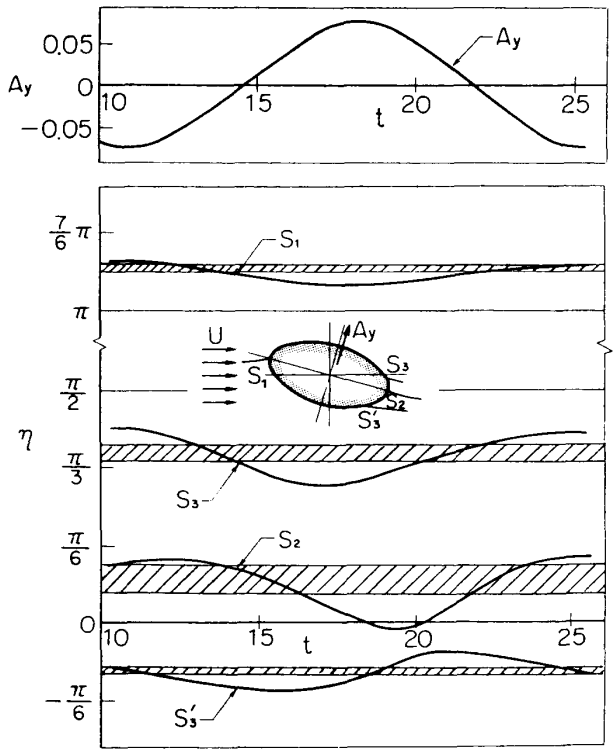

FIG. 10. The behaviours of the points where the viscous shear stress vanishes on the transversally oscillating elliptic cylinder with the thickness ratio of 50% at $Re=80$, $\alpha=15°$, $k=1.0$ and $\delta/c=10\%$.
▨ denotes the amplitude of the fluctuation due to the Karman vortex street.

where the viscous shear stress vanishes, is shown in Fig. 10. As the Karman vortex street appears in the wake of the stationary elliptic cylinder as already shown in Fig. 1 (b), the width of the movement of these points due to this vortex street is shown by the shaded areas in Fig. 10, where η is the value defined by equation (1) in the elliptic coordinates.

When this cylinder is oscillating under the reduced frequeny $k=1.0$ and the amplitude of displacement $\delta/c=10\%$, these points S_1, S_2, S_3 and $S_{3'}$ move along the surface about the shaded areas shown for the stationary case, by 1.5%, 5.5%, 7.4% and 2% of the chord-length in amplitude, respectively. The movement of these points is much more pronounced than either that due to the Karman vortex street or that for the case of the 20% oscillating elliptic cylinder.

4. Experimental Apparatus

A series of experiments are carried out to measure aerodynamic forces and pressures exerted on an oscillating elliptic cylinder operating over a relatively wide range of Reynolds number. In these experiments, we use the same experimental apparatus used for a circular cylinder as described

in detail in a previous paper, Okajima, Takata and Asanuma (1975). This apparatus satisfactorily fulfills the requirements of two-dimensional flow, low level of disturbance, accuracy of measurement and other criteria, as it adopts the system towing the test cylinder in a still liquid, either water or oil.

4-1. Tank and measuring carriage

As shown in Fig. 11, the experimental apparatus includes a tank ①, a measuring carriage ③ and other such items as were used in the case of the circular cylinder. The tank is 0.7m wide, 0.4m deep and about 10m long and is filled with water or oil. The measuring carriage slides on tracks ② and is towed by ropes ④ which are wound on a drum driven by a variable-speed electric motor. The test cylinder ⑤ is suspended vertically downward from this carriage and is forced to oscillate transversally in the direction normal to the chord-line of the cylinder with arbitrary frequency and amplitude by an oscillator which consists of a small variable-speed electric motor ⑥, a gear train ⑦, a synchoro-belt ⑧, and a crank wheel and scotch yoke mechanism ⑨.

Several different experimental conditions can be obtained as follows: Reynolds number may be changed by varying the towing speed or using different fluids such as water or oil, the oscillatory amplitude of test cylinder may be changed by using a different crank wheel and its oscillatory frequency may be done by varying the speed of the oscillator motor. The available

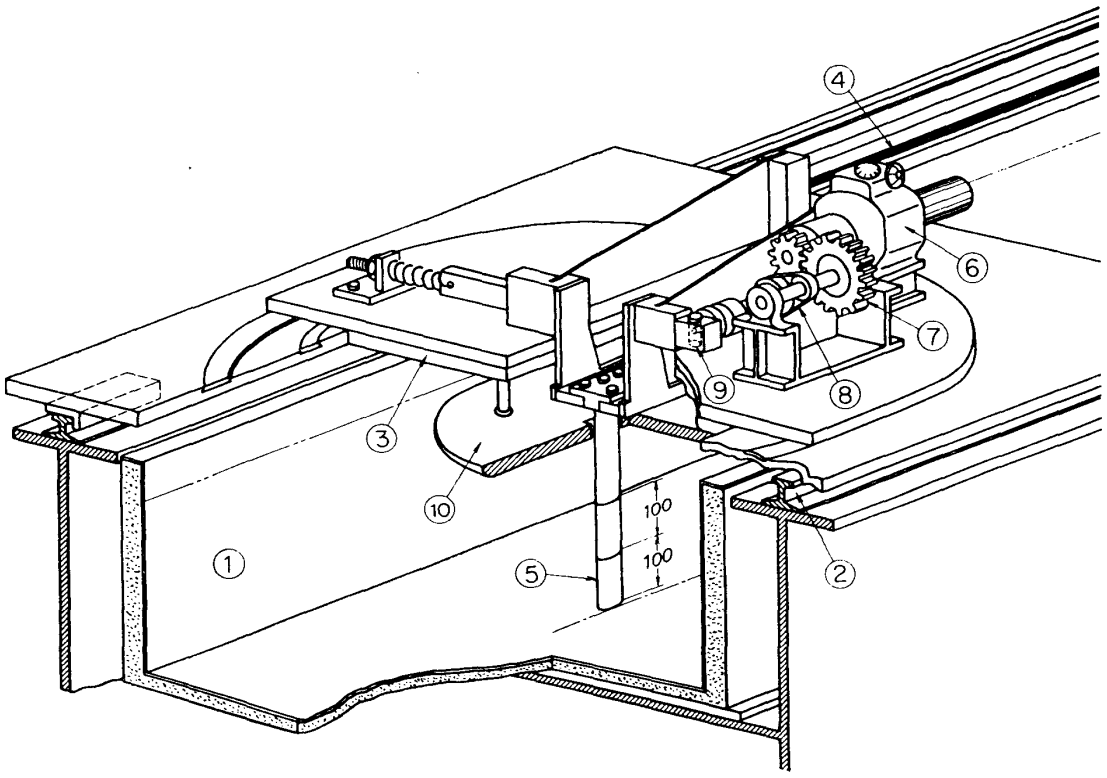

FIG. 11. Experimental apparatus.

Reynolds numbers are thus about $Re=40$ to 200 for oil and $Re=1500$ to 20000 for water.

The free surface effects are eliminated by mounting a circular plastic dics ⑩ (500mm diameter) at the top of the test cylinder which just contacts the free surface of liquid, and all of the measurements are made on the central part of the test cylinder, as described in the following section.

4-2. Test cylinder

Rather than constructing one very complex test elliptic cylinder for making all test measurement, we prepared three different cylinders in order to measure normal force, moment and pressure independently. All of these test cylinders are 50mm in chord-length and 370mm in span-length, with a thickness ratio of 20%. The two for measuring normal force and moment consist of three sections in the spanwise direction, only the central section of which is used for measurements so as to eliminate the effect of the three-dimensionality of flow due to surface wave, end-clearance and so on as much as possible. It is 100mm in span-length, made of plastic and hollowed out to reduce its inertia and is suspended from the upper dummy section of the test cylinder through two parallel leaf springs on which four strain gauges are mounted to form Wheatstone bridge. These leaf springs are flexible in only one direction and respond either to a force perpendicular to the chord of the elliptic cylinder or to a moment about the midchord point. The natural frequency of the central test section suspended by leaf springs is estimated to be over 30Hz in water. The present experiment is conducted in a range of driving frequency of the cylinder of less than 2Hz. Thus there should be no difficulty due to the above-mentioned natural frequency. The upper and the lower sections of the cylinder are 170mm and 100mm long in span and fastened to each other by two parallel connecting rods. The gaps between these three sections are adjusted to be 0.2mm or less; they were also preliminarilly checked to have no perceptible influence on the measurements.

The test cylinder for the measurement of pressure have seven taps along the chord on one side of the surface. Pipes 3mm in diameter are placed inside the cylinder filled with water or oil and go from the pressure taps to a pressure transducer through a changeover cock. The pressure of the of the individual taps can be measured in separate runs, with satisfactory accuracy and response by means of the transducer which is sufficiently sensitive to respond to a change in pressure of 1/10mm water.

5. Results of Experiment

Results of the experiment obtained with the model of the same geometry and under the same condition as the case of the numerical calculation are compared with the calculated results at low Reynolds numbers. Further, experimental results are presented to provide more information over the range of Reynolds number up to 20000.

5-1. Comparison between the experimental results and the calculated results

Fig. 12 shows the experimental results of the static pressure distribution $\overline{C}_p$ along the chord x/c for example, in the case of the stationary elliptic cylinder with the angle of attack $\alpha=0°$ and 15° at Reynolds number $Re=80$, compared with the results by the numerical calculation. In this figure, the pressure $\overline{C}_p$ is set on the basis of that of trailing edge and the lowest value of the pressure is detected to be near the middle point of the chord for $\alpha=0°$ and in the vicinity of the leading edge on the upper surface for $\alpha=15°$. It is remarkable that this figure indicates a good agreement between the experimental and the calculated results on both the upper and the lower surfaces of the cylinder. Fig. 13 summarizes both the experimental and

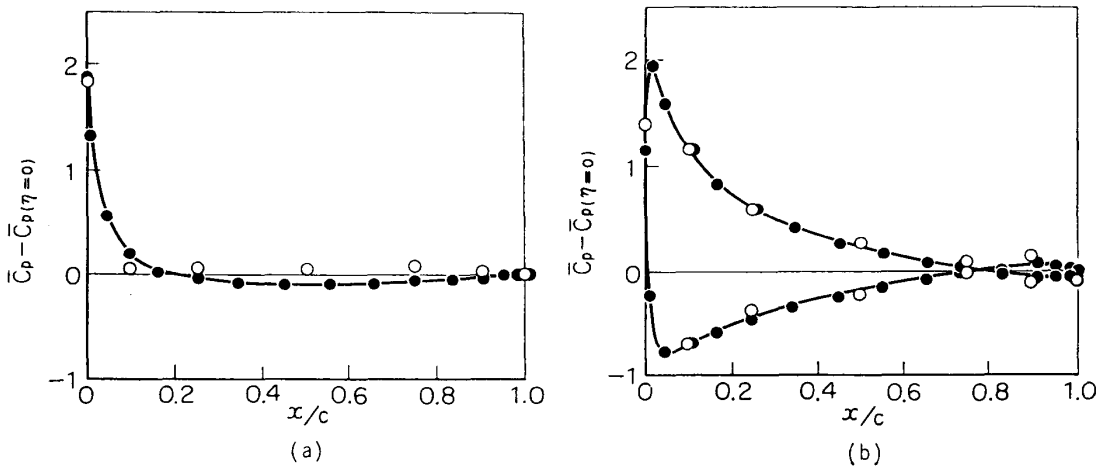

FIG. 12. Pressure distributions on the surface of the stationary elliptic cylinder with the thickness ratio of 20% at $Re=80$, $\alpha=0°$ and 15°.
-●-, Numerical solutions; ○, Experimental measurements.

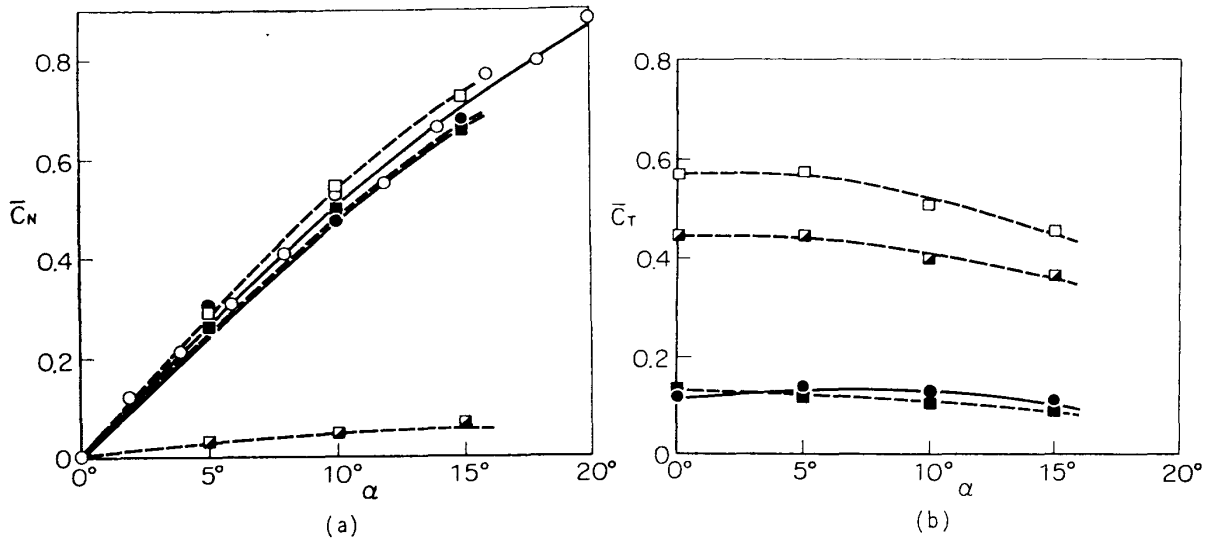

FIG. 13. Normal and tangential forces of the stationary elliptic cylinder with the thickness ratio of 20% at $Re=80$.
Numerical solutions: --□--, C_N, C_T; --■--, C_{NP}, C_{TP}; --◪--, C_{NS}, C_{TS}.
Experimental measurements: -○-, C_N, C_T; -●-, C_{NP}, C_{TP}.

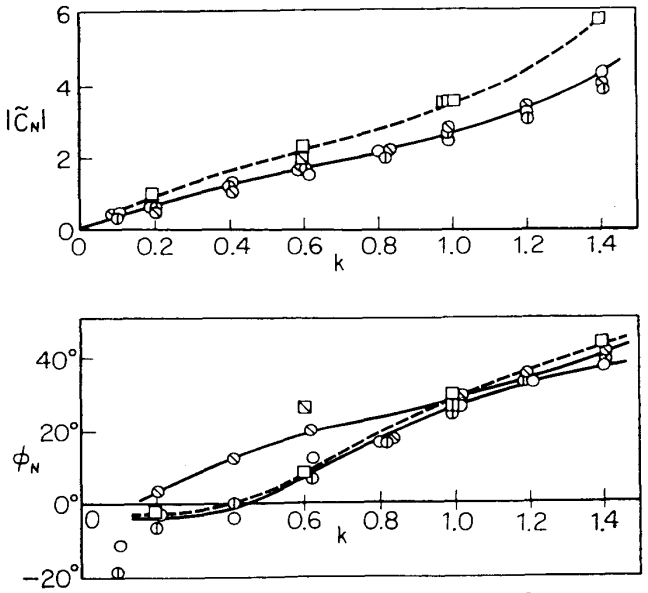

(a) Fluctuating normal force, Re=40

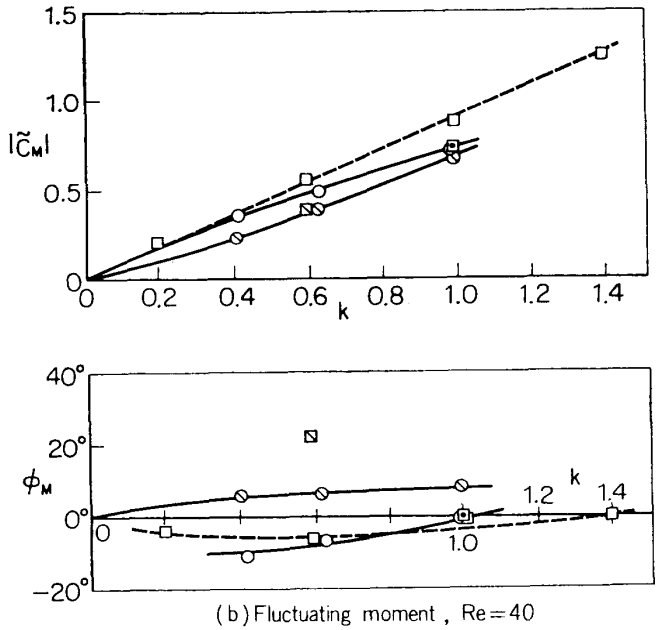

(b) Fluctuating moment, Re=40

FIG. 14-1. Experimental and calculated results of the fluctuating normal force and moment of the transversally oscillating elliptic cylinder with the thickness ratio of 20% at $Re=40$. Experimental measurements: -○-, $\alpha=0°$; ◑, $\alpha=5°$; -⊘-, $\alpha=15°$; -⊘-, $\alpha=20°$. Numerical solutions: --□--, $\alpha=0°$; --⊡--, $\alpha=0°$ by fine mesh; ◫, $\alpha=5°$; ◪, $\alpha=15°$; ◪, $\alpha=20°$.

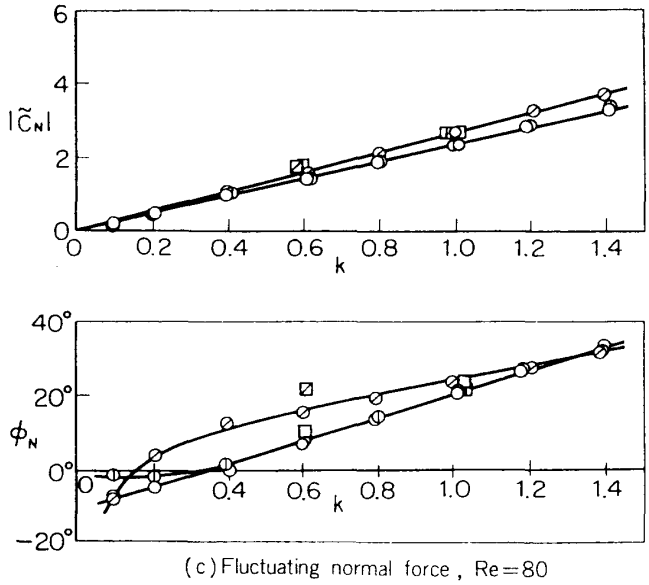

(c) Fluctuating normal force, Re=80

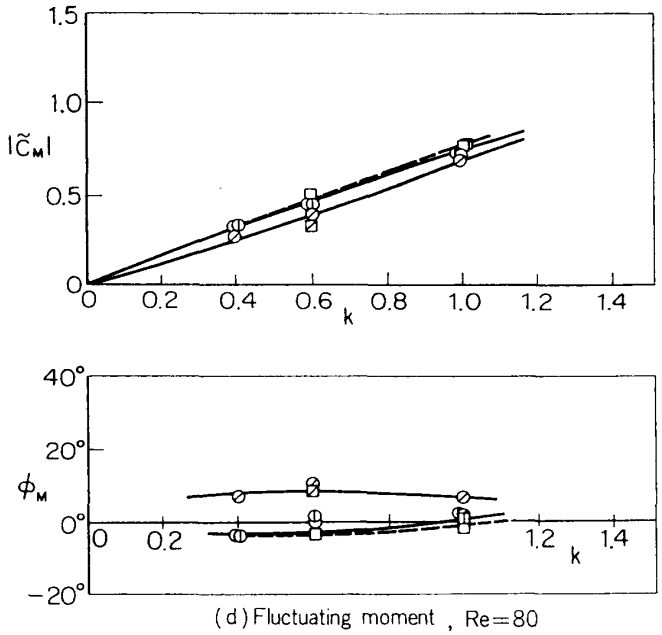

(d) Fluctuating moment, Re=80

FIG. 14–2. Experimental and calculated results of the fluctuating normal force and moment of the transversally oscillating elliptic cylinder with the thickness ratio of 20% at Re=80; symbols as Fig. 14–1.

the calculated values of the normal and the tangential forces $\overline{C}_N$, $\overline{C}_T$ against the angle of attack α at $Re=80$. The experimental values of component due to pressure are obtained by the numerical integration of the measured pressure distributions as in Fig. 12. It is clearly recognized that the calculated results shown by the broken lines agree well with the experimental ones shown by the solid lines.

Figs. 14 (a) to 14 (d) give a comparison between the experimental and the calculated results for the amplitudes and phases of the fluctuating normal force $\tilde{C}_N$ and the fluctuating moment $\tilde{C}_M$ acting on the oscillating cylinder for the cace of $Re=40$ and 80, $\alpha=0°$ to 20°. In these figures, the amplitudes and phases of the experimental and the calculated values of $\tilde{C}_N$ and $\tilde{C}_M$ are found to be in good agreement. However, there is some discrepancy in the amplitude $|\tilde{C}_N|$ at $Re=40$ and $k=1.4$. This may be due to rather poor accuracy in the calculation for the case of very fast oscillation. Nevertheless, as a whole, the over-all agreement between the experimental and the calculated results for the oscillating cylinder is remarkably good.

5-2. *Experimental results for higher Reynolds numbers*

(a) Stationary normal forces

Fig. 15 gives the characteristic curves of the normal force $\overline{C}_N$ measured in water and oil for high Reynolds numbers, $Re=5000$ to 20000 and low Reynolds numbers, $Re=40$ to 200, respectively. In this figure we can see the so-called stall characteristic at high Reynolds numbers, as indicated by

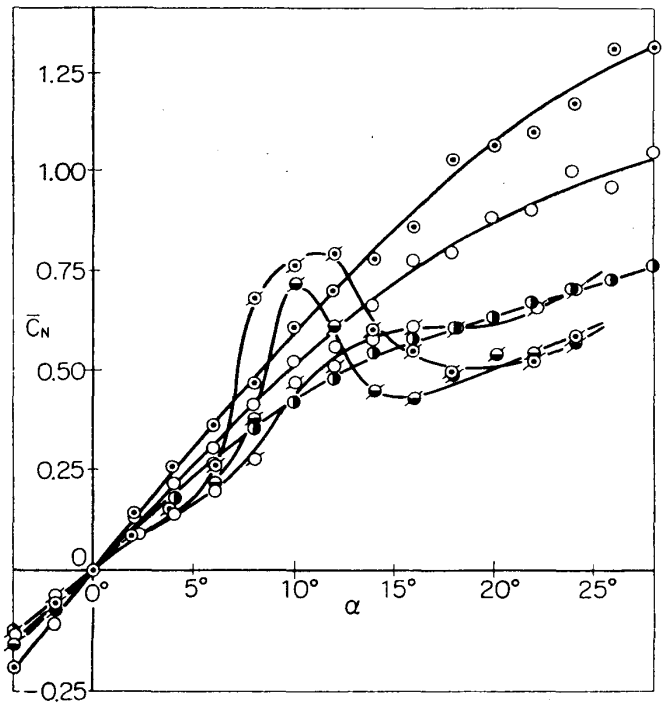

FIG. 15. Normal forces of the stationary elliptic cylinder with the thickness ratio of 20%.
⊙, $Re=40$; ○, $Re=80$; ◑, $Re=200$; ⌀, $Re=5000$; ⌀, $Re=10000$; ⌀, $Re=20000$.

an abrupt decrease of $\overline{C}_N$ as the angle of attack α is increased. At the leading edge of the cylinder, laminar separation of flow can be observed to occur by means of the visualization technique. At low Reynolds numbers, however, there is little or no sign of stall characteristic, that is, the parameter $\overline{C}_N$ increases monotonically with an increase in the angle of attack, and the lower Reynolds number is, the larger the parameter $\overline{C}_N$ is.

(b) Fluctuating normal forces

In the range of Reynolds number $Re=40$ to 15000 and reduced frequency $k=0.1$ to 1.4, the experimental results of the fluctuating normal force for angles of attack of $\alpha=0°$ and 15° are presented in Figs. 16 (a) and 16 (b) respectively. In the region of the non-stalled state, e.g. $\alpha=0°$, the fluctuating normal forces $\tilde{C}_N$ are essentially independent of Reynolds number and lie almost on a single curve. Their magnitudes are always smaller than the values of the potential flutter theory which are shown by a broken line. This decrease in the non-stalled state below that predicted by theory can be attributed to the effect of fluid viscosity, which makes the slopes of the static

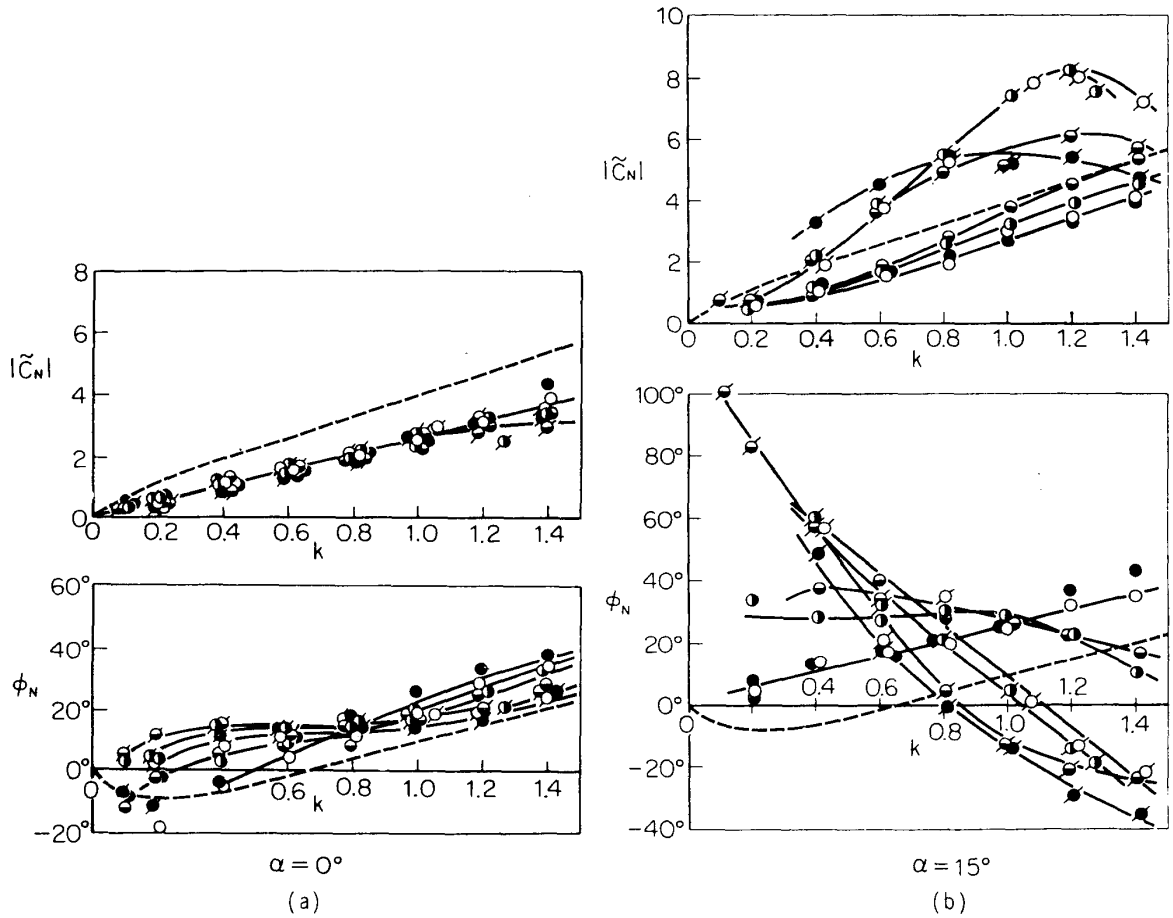

FIG. 16. Fluctuating normal forces of the transversally oscillating elliptic cylinder with the thicknessratio of 20% at $\alpha=0°$ and 15°.
●, $Re=40$; ○, $Re=80$; ◑, $Re=200$; ◒, $Re=400$; ◌, $Re=5000$; ◑, $Re=7000$; ◒, $Re=10000$; ●, $Re=15000$; ----, inviscid flutter theory for flat plate.

normal forces smaller than 2π as shown in Fig. 15, where at $\alpha=0°$, $\partial\bar{C}_N/\partial\alpha\simeq\pi$ for the lower Reynolds numbers and $\partial\bar{C}_N/\partial\alpha\simeq 0.6\pi$ for the higher Reynolds numbers. So, at rather small angles of attack, the fluctuating normal forces may be predicted approximately by using these values of the slopes of static normal forces which can be obtained from Fig. 15, instead of the value of 2π from the potential flutter theory. In the range of higher Reynolds numbers ($Re=5000$ to 15000) as shown in Fig. 16 (b), when the elliptic cylinder oscillates at an angle of attack in the stalled region, e.g. $\alpha=15°$, the amplitudes of the fluctuating normal forces may increase abruptly with an increase in reduced frequency, in spite of the negative slope of the static normal forces. Referring to Fig. 16 (b), it is seen that for the low reduced frequencies, the phases of the fluctuating normal forces reach as much as 100° ahead of those of the quasi-steady normal force. This can be explained by the quasi-steady consideration as follows: when the elliptic cylinder

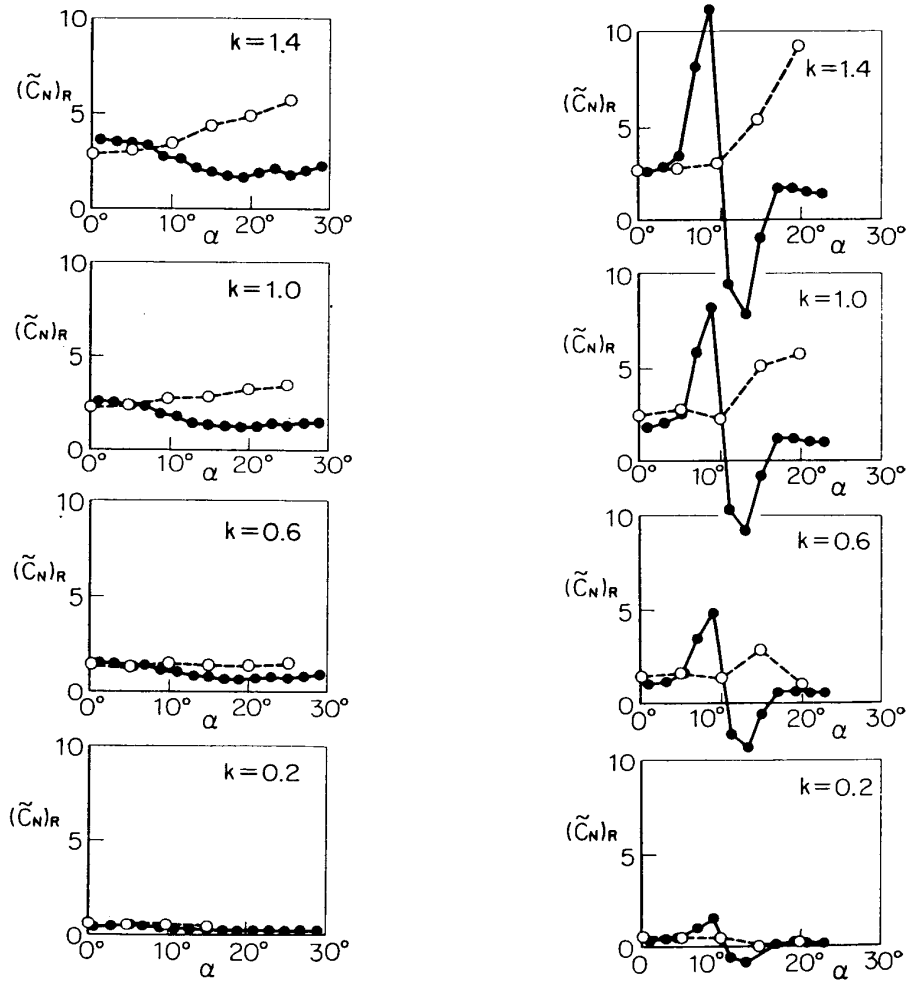

(a) Re=200 (b) Re=10000

FIG. 17. The in-phase components of fluctuating normal force of the transversally oscillating elliptic cylinder with the thickness ratio of 20%.
--○--, $(\tilde{C}_N)_R$; -●-, $(\tilde{C}_N)_{QS}=k(\cos\alpha\cdot\partial\bar{C}_N/\partial\alpha+2\bar{C}_N\sin\alpha)$.

oscillates with very low frequencies, the normal force exerted on it may be nearly proportional to the slope of the static normal force, so that in the stalled region where this slope becomes negative the fluctuation of the normal forces and the oscillatory velocity of the cylinder are naturally out of phase, each other and its phase difference is ahead of that of the force exerted in the non-stalled state. As the reduced frequency becomes fast, however, the viscous effect is much more complicated and brings about a change not only in the amplitude of the fluctuating normal forces but also in their phase.

We examine the effects of the angle of attack and Reynolds number on the force exerted on the oscillating cylinder. In Fig. 17, both the in-phase component $(\tilde{C}_N)_R=\tilde{C}_N\cos\phi_N$ of the fluctuating normal forces with the oscillatory velocity which is the so-called aerodynamic damping coefficient and the quasi-steady aerodynamic damping coefficient $(\tilde{C}_N)_{QS}$ calculated by $(\tilde{C}_N)_{QS}=k(\partial\bar{C}_N/\partial\alpha\cos\alpha+2\bar{C}_N\sin\alpha)$ are plotted for comparison, against the angle of attack α as a parameter of Reynolds number. This figure shows that at a small angle of attack, $\alpha=0°$ to 5°, both results are in essential agreement, but with an increase in the angle of attack the two become noticeably different. $(\tilde{C}_N)_R$ abruptly increases with the angle of attack α, even if the Reynolds number is so small that there is little sign of stall characteristic in the static curve of the normal force $\bar{C}_N$, as shown in Fig. 15, e.g. $Re=200$. Furthermore, when the cylinder operates in the stalled state for both large Reynolds number and large angle of attack such as $Re=10000$ and $\alpha=12°$, $(\tilde{C}_N)_R$ is found to take positive values which are considerably larger than those for $(\tilde{C}_N)_{QS}$ which is often negative. This

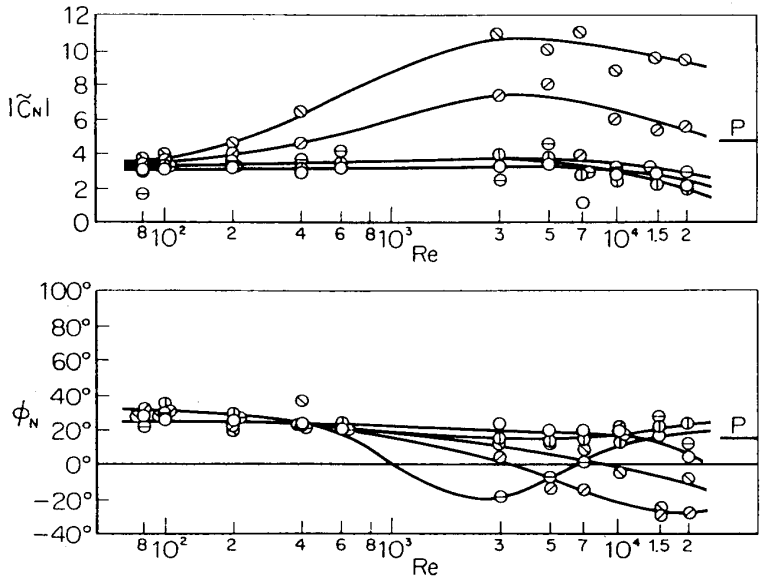

FIG. 18. Fluctuating nornal force of the transversally oscillating elliptic cylinder with the thickness ratio of 20%, with reduced frequency $k=1.2$.
○, $\alpha=0°$; ◑, $\alpha=5°$; ⊖, $\alpha=10°$; ⊘, $\alpha=15°$; ⊗, $\alpha=20°$.
P, inviscid flutter theory for flat plate.

discrepancy, also, can be attributed to the viscous effect of the flow around the oscillating cylinder.

Fig. 18 illustrates the typical variations of the amplitude and phase of the fluctuating normal force with the Reynolds number, as a parameter of the angle of attack, at the constant reduced frequency, i.e. $k=1.2$. In the case of a small angle of attack, the region of separated flow is confined to only the vicinity of the trailing edge of the elliptic cylinder and the amplitude and phase of the fluctuating normal force, therefore, keep the constant value in the wide range of Reynolds number, in spite of such fast frequency as $k=1.2$.

However, increasing the angle of attack, we can see more pronounced dependence of the fluctuating normal force on Reynolds number. The increase of the angle of attack and Reynolds number causes the boundary layer on the upper surface of the elliptic cylinder to separate near the leading edge, and the amplitude of the normal force becomes over twice as much as the value of the potential theory accompanied with the phase-

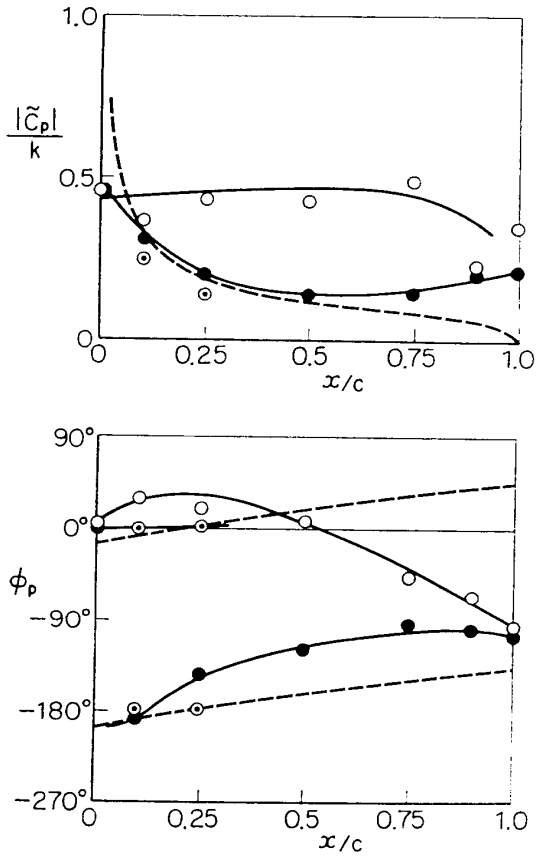

FIG. 19. The amplitude and phase of fluctuating pressures along the surface of the transversally oscillating elliptic cylinder with the thickness ratio of 20% at $Re=10000$ and $k=0.8$.
⊙, $\alpha=0°$; -○-, $\alpha=15°$, upper side of the cylinder; -●-, $\alpha=15$, lower side of the cylinder; ----, inviscid flutter theory for flat plate.

lagging as shown in Fig. 18.

(c) Fluctuating pressure on the elliptic cylinder at $Re=10000$

Fig. 19 shows the amplitude and phase of the fluctuating pressure on the surface of the elliptic cylinder for the case of $\alpha=0°$ (non-stalling) or $\alpha=15°$ (stalling) at $Re=10000$ and $k=0.8$. It is seen from this figure that in the non-stalled state the experimental values have the same tendency as those of the potential flutter theory shown by broken lines, except for smaller amplitudes in the former. In the stalled state, however, the amplitudes of the pressures become uniformly as large as that of the leading edge ($x/c=0$) over the whole upper surface of the elliptic cylinder on which the boundary layer is observed to be separating. Furthermore, it may be noticed that the amplitude of the pressure at the trailing edge is ($x/c=1$) not zero but some finite value such that the phases of pressures on upper and lower surfaces coincide with each other at that edge. Finally, Fig. 20 presents a comparison between the values of the normal force measured directly by the strain-gauge method and those of the component of the normal force due to pressure obtained from the preceding pressure distribution, since the component of the normal force due to skin friction seems

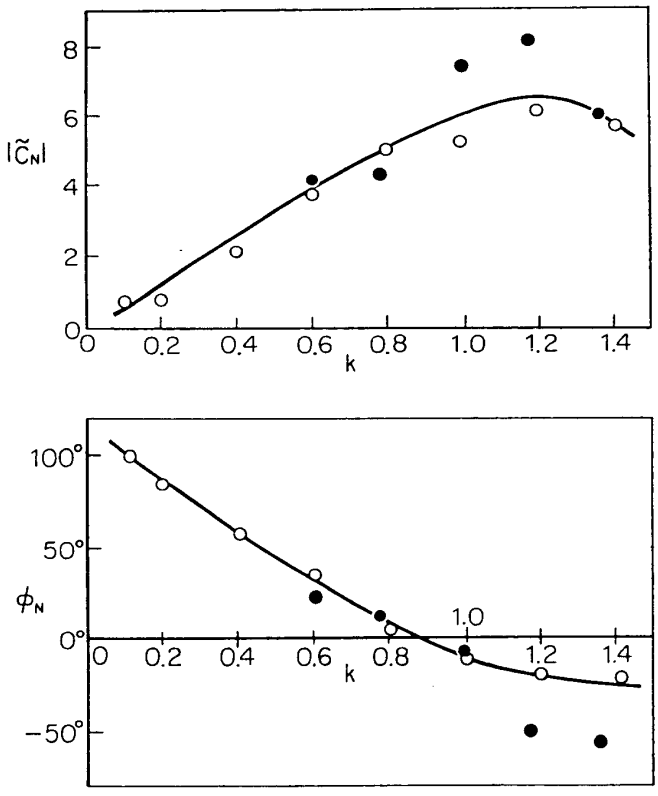

FIG. 20. Comparison between the values of the fluctuating normal force measured by the pressure pick-up and those by the strain gauge at $Re=10000$, $\alpha=15°$ and $k=1.0$.
○, $\tilde{C}_N$ measured by the strain gauge; ●, $\tilde{C}_{NP}$ measured by the pressure pick-up.

to be negligible at such high Reynolds number. The measured values of pressure around the cylinder are so small in number, i.e. 12, that the accuracy of the latter method is not satisfactory. The results measured by two different methods are, however, seen almost to agree in this figure, which indicates that the two kinds of methods verify one another.

6. Concluding Remarks

By similar methods to that for the case of circular cylinder, we have numerically calculated the viscous flow around both stationary and transversally oscillating elliptic cylinders at $Re=40$ and 80, and also measured aerodynamic forces and pressure in the range of Reynolds number, $Re=40$ to 20000. The time-variation of the flow configurations and the aerodynamic parameters are calculated numerically by a finite difference method. For the stationary case of the elliptic cylinder with the thickness ratio of 20%, the flow separation is hardly observed on the surface and the point of downstream stagnation where the shear stress vanishes stays very near the vicinity of the trailing edge, in spite of its round edge, for such small Reynolds number as 40 or 80, and a high angle of attack of $\alpha=20°$. Further a periodic transversal oscillation of this elliptic cylinder has no great affect on the flow around the cylinder operating in the ranges of Reynolds number $Re=40$ and 80, angle of attack $\alpha=0°$ to 20° and the oscillatory frequency $k=0.1$ to 1.4. However, it causes the point of downstream stagnation to move periodically with small amplitude about its location for stationary case, with some phase lead difference.

For the stationary elliptic cylinder with the thickness ratio of 50%, it is found that a standing twin vortex ($\alpha=0°$) or the Karman vortex street ($\alpha=15°$) forms behind the cylinder accompanied with separation of the boundary layer. The transversal oscillation of the 50% elliptic cylinder induces the vortex street to shed behind the cylinder with the same frequency as this oscillation and exhibits a sign of the vortex-excitation phenomenon.

Aerodynamic parameters measured with satisfactory accuracy are compared with the values by the numerical calculation and it is confirmed that there is a good agreement between them for both stationary and oscillating elliptic cylinders.

Furthermore, some information is supplied from the experimental results in the relatively wide range of Reynolds number. When an elliptic cylinder operates in the non-stalled state, the fluctuating components of the normal force and the moment are found to be weakly dependent on Reynolds number, in the range of $Re=40$ to 20000. The shape of the curves, but not the magnitudes, agree with the values obtained with the inviscid potential theory. On the other hand, when the cylinder on which the boundary layer separates in the vicinity of the leading edge operates in the stalled state, the pressures on the upper surface of the oscillating cylinder are observed to fluctuate in a sinusoidal fashion with a large amplitude. In addition, the

amplitudes of the fluctuating aerodynamic parameters become considerably larger than values inferred by the quasi-steady consideration, accompanied by a great change in the phase shift.

Therefore, in a small angle of attack, the effects of Reynolds number is not seen on the fluctuating force, but within large angle of attack, there arises the phenomenon of the stalling, and Reynolds number has pronounced effects on the fluctuating force.

Department of Jet Propulsion
Institute of Space and Aeronautical Science
University of Tokyo
July 30, 1975

References

Chu, W., 1962: J. Aero. Sci. **29**, 781.

Lugt, H. J. and Haussling, H. J., 1972: Naval Ship Research and Development Center, Report 3748.

Miyagi, T., 1964: J. Phys. Soc. Japan, **19**, 6, 1063.

Moore, F. K., 1955: NACA TN, 3751.

Okajima, A., Takata, H. and Asanuma, T., 1975: Inst. Space and Aero. Sci. Univ. Tokyo, Report 532.

Shen, S. F. and Crimi, P., 1965: J. Fluid Mech. **23**, 585.

Wang, C. Y., 1966: M. I. T. Fluid Dynamics Research Laboratory Report, 66-4, and also, 1967: J. appl. Mech. ASME, **34**, 4, 823.